JACS
JOURNAL OF THE AMERICAN CHEMICAL SOCIETY
pubs.acs.org/JACS
Article

Structure and Properties of $Cs_7(H_4PO_4)(H_2PO_4)_8$: A New Superprotonic Solid Acid Featuring the Unusual Polycation $(H_4PO_4)^+$

Louis S. Wang, Sawankumar V. Patel, Sheel S. Sanghvi, Yan-Yan Hu, and Sossina M. Haile*

Cite This: J. Am. Chem. Soc. 2020, 142, 19992–20001

ABSTRACT: We report the discovery of a new superprotonic compound, $Cs_7(H_4PO_4)(H_2PO_4)_8$, or CPP, which forms at elevated temperatures from the reaction of CsH_2PO_4 and $CsH_5(PO_4)_2$. The structure, solved using high-temperature single-crystal X-ray diffraction and confirmed by high-temperature ^{31}P NMR spectroscopy, crystallizes in space group $Pm\bar{3}n$ and has a lattice constant of 20.1994(9) Å at 130 °C. The unit cell resembles a 4 × 4 × 4 superstructure of superprotonic CsH_2PO_4, but features an extraordinary chemical moiety, rotationally disordered $H_4PO_4^+$ cations, which periodically occupy one of every eight cation sites. The influence of this remarkable cation on the structure, thermodynamics, and proton transport properties of the CPP phase is discussed. Notably, CPP forms at a temperature of 90 °C, much lower than the superprotonic transition temperature of 228 °C of CsH_2PO_4, and the compound does not appear to have an ordered, low-temperature form. Under nominally dry conditions, the material is stable against dehydration to ∼151 °C, and this results in a particularly wide region of stability of a superprotonic material in the absence of active humidification. The conductivity of $Cs_7(H_4PO_4)(H_2PO_4)_8$ is moderate, 5.8×10^{-4} S cm^{-1} at 140 °C, but appears nevertheless facilitated by polyanion $(H_2PO_4^-)$ group reorientation.

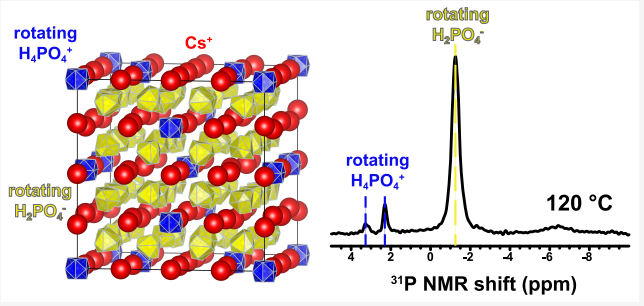

1. INTRODUCTION

Superprotonic solid acids are crystalline phases characterized by orientationally disordered acidic oxyanion groups that undergo rapid reorientation around fixed central atoms. The coupling of this motion with interoxyanion proton hopping produces a variant of the Grotthuss mechanism and results in high proton mobilities along with long-range proton transport. Among the known superprotonic conductors, cesium dihydrogen phosphate, CsH_2PO_4, or CDP, is particularly suited for implementation as a fuel cell electrolyte, because, in addition to its high proton conductivity, it displays chemical stability against reaction with both oxygen and hydrogen. Accordingly, CDP has been heavily studied in this capacity.[1−7] The superprotonic phase of CDP features a CsCl-like arrangement of Cs cations and orientationally disordered phosphate anions. The phase occurs at temperatures above 228 °C, but requires active humidification ($\sim p H_2O$ > 0.2 atm) to prevent dehydration.[8] Several authors have sought to use chemical modification to expand the stability window of the superprotonic CDP phase and reduce the humidification requirements. The various approaches have included cation site doping with Rb, K,[9] NH_4,[10] and Ba,[11] as well as "heterogeneous" doping by introducing components such as $Cs_2HPO_4{\cdot}H_2O$,[12] $Ba(H_2PO_4)_2$,[13] SiO_2,[14] SiP_2O_7,[15] and even $Cs_5H_5N_5O$.[16] Of particular relevance to the present work is a study that was conducted by Ponomareva et al. on the impact of Cs deficiency on CDP, achieved by the addition of excess $CsH_5(PO_4)_2$ or H_3PO_4.[17] While the authors reported unusually high proton conductivities at temperatures below the superprotonic transition temperature of CDP, the phase behavior was not characterized.

Here we report the discovery of a new superprotonic compound: heptacesium tetra-hydroxyphosphonium octa-dihydrogenphosphate, $Cs_7(H_4PO_4)(H_2PO_4)_8$, or CPP. The compound was revealed as part of a systematic study of the phase behavior in the CDP−$CsH_5(PO_4)_2$ system. As described below, CPP is thermodynamically stable at temperatures as high as 151 °C even without humidification and can be produced by either solid-state reaction or high-temperature crystallization from aqueous solution. The structure of $Cs_7(H_4PO_4)(H_2PO_4)_8$ is rather remarkable in that it contains the tetra-hydroxyphosphonium cation, $H_4PO_4^+$. This polycation is an exceptionally rare species, especially in crystalline solids. The first supported report of its occurrence in a crystalline material was in $H_4PO_4{\cdot}ClO_4$, but the structure was

Received: August 17, 2020
Published: November 12, 2020

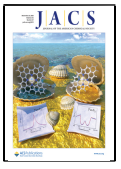

https://dx.doi.org/10.1021/jacs.0c08870
J. Am. Chem. Soc. 2020, 142, 19992−20001

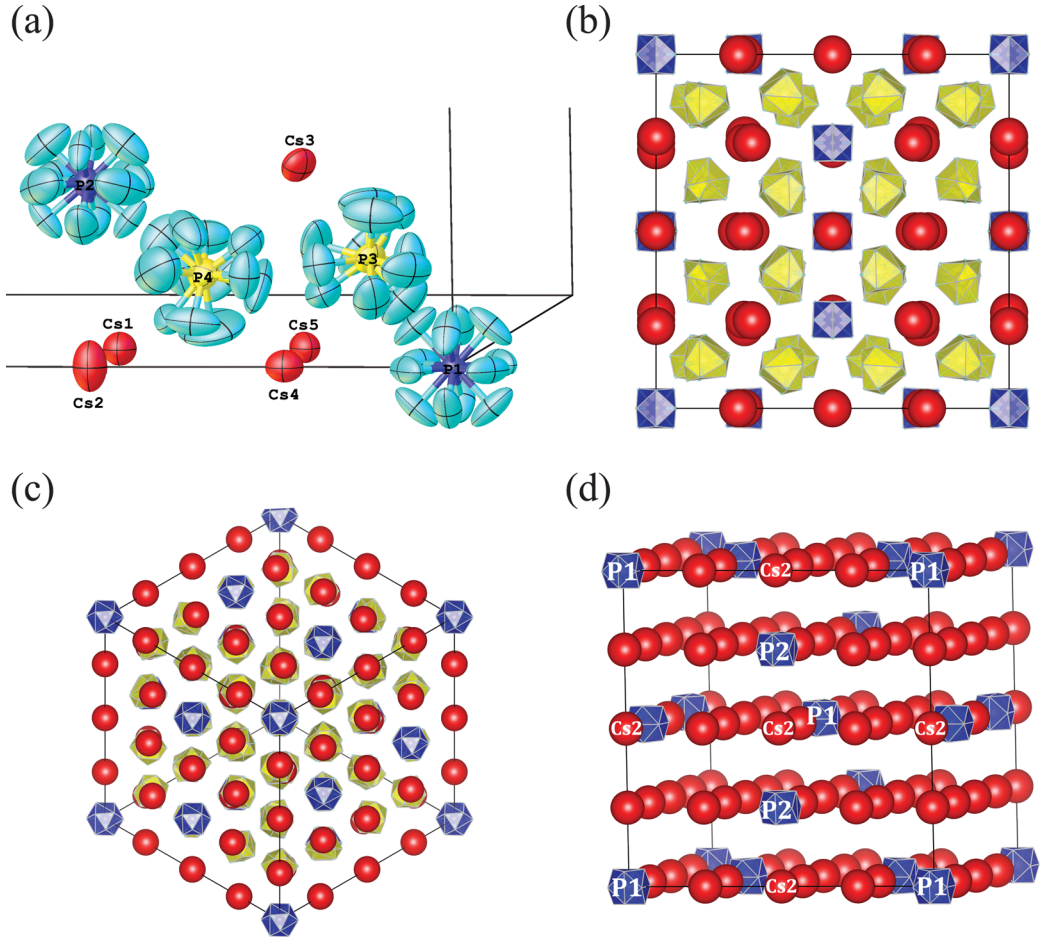

Figure 1. Crystal structure of $Cs_7(H_4PO_4)(H_2PO_4)_8$: (a) rendition of the asymmetric unit, depicting atomic displacements; (b) projection of the unit cell along [100]; (c) projection along [111]; and (d) idealized depiction of the arrangement of species on the cation sites. In (a) unlabeled atoms are oxygen; in (b), (c), and (d), H_nPO_4 groups are shown as polyhedra, with those about P1 and P2, the polycations, shown in blue, and those about P3 and P4, the polyanions (not depicted in (d)), shown in yellow; Cs atoms are shown in red.

not characterized.[18] To our knowledge, the only prior crystallographic studies of the $H_4PO_4^+$ ion have been in KH_2PO_4,[19] a result that has been questioned,[20] and in $P(OH)_4^+MF_6^-$ (M = As, Sb).[20] In both the crystalline and the liquid systems, the occurrence of tetra-hydroxyphosphonium is attributed to the presence of strong acids capable of donating protons to the phosphate group.[20−23] The absence of such groups in $Cs_7(H_4PO_4)(H_2PO_4)_8$ renders the present discovery particularly surprising. Here we evaluate the proton transport, thermodynamics, and stability of this new compound.

2. CRYSTAL SYNTHESIS AND STRUCTURE DETERMINATION

2.1. Methods. The compounds CsH_2PO_4 (CDP) and $CsH_5(PO_4)_2$ were independently prepared as precursors for the synthesis of CPP. Crystals of both materials were grown from the evaporation of aqueous solutions of stoichiometric quantities of Cs_2CO_3 and phosphoric acid at ambient conditions. Stoichiometric mixtures of CDP and $CsH_5(PO_4)_2$ (5:2 molar ratio) were homogenized by grinding, pressed into dense compacts at 275 MPa, and annealed at 130 °C for 3 days under dry N_2 gas flow. After being annealed, the densified samples were immediately transferred to an N_2 atmosphere glovebox and further ground into a powder. As shown below, no reaction between CDP and $CsH_5(PO_4)_2$ occurs throughout these processing steps. All subsequent references to powder precursor samples are to materials prepared in this way.

Crystals of $Cs_7(H_4PO_4)(H_2PO_4)_8$ were grown for single-crystal X-ray diffraction from the powder precursor samples using a high-temperature deliquescence and crystallization procedure.[24] Approximately 1 g of the powder sample of CDP and $CsH_5(PO_4)_2$ was heated to 102 °C in a tube furnace. A highly humidified gas stream (pH_2O = ∼0.93 atm) was then supplied to the sample, achieved by bubbling 40 sccm (standard cubic cm per min) Ar through 98 °C water. The sample was held under this condition for 6 h to achieve complete deliquescence, forming a concentrated liquid solution. The temperature was then slowly increased to 130 °C in 5 °C steps with a 2 h hold at each step, while maintaining the humidified atmosphere. The water gradually evaporated, and the target phase crystallized. The crystals were stored and transported to the diffractometer in a small mobile oven kept at 130 °C. During the diffraction measurements, the selected crystal was preserved by a flow of argon heated to 130 °C. To maintain the high-temperature structure, exposure to ambient temperature was limited to only the steps of crystal selection and mounting.

Single-crystal X-ray diffraction data for structure solution were collected using Mo Kα radiation (λ = 0.71073 Å) on a

https://dx.doi.org/10.1021/jacs.0c08870
J. Am. Chem. Soc. 2020, 142, 19992−20001

Bruker Kappa APEX with a CCD (charge-coupled device) area detector. Absorption corrections were applied using SADABS-2016/2. A total of 9772 reflections were captured, from which a cubic unit cell with a = 20.1994(9) Å was established. The space group was determined as $Pm\bar{3}n$ using Xprep (SHELX).[25] The formula unit was defined as 7 cesium atoms, 9 phosphorus atoms, and 36 oxygen atoms, with 8 formula units per unit cell, where the protons have been left out of the structure refinement.

The structure of CPP was solved by direct methods (SHELXS) and refined by least-squares minimization (SHELXL).[25] Direct structure solution generated an asymmetric unit with five Cs and three P atom sites. An additional P atom site was subsequently identified, producing, as a consequence of the site multiplicities, the anticipated Cs:P ratio of 7:9. All atoms were initially refined with isotropic thermal displacements. Oxygen positions were found using successive Fourier difference maps, while restraining oxygen thermal displacements to U_{iso} = 0.08 Å^2 and P−O bond lengths to 1.58 Å. Significant attention was paid to establishing the oxygen site occupancies during structure refinement. Ultimately, a value of 1/3 for all oxygen sites produced the most sensible coordination environments and overall stoichiometry. In the final stages of the analysis, variable anisotropic thermal displacement parameters were introduced, and the structure was refined until convergence. Final respective R_1 and wR_2 values of 4.28% and 12.12% were achieved. Details of the diffraction experiment, structure solution, and refinement are summarized in Table S-1.

Further structural characterization was carried out by high-temperature solid-state ^{1}H and ^{31}P magic angle spinning (MAS) nuclear magnetic resonance (NMR) spectroscopy, which also provided insight into the material dynamics. MAS NMR spectra were collected on a Bruker spectrometer at a Larmor frequency of 300 MHz for ^{1}H and 121 MHz for ^{31}P, using a 4 mm Bruker MAS probe at a sample spinning rate of 8 kHz. A powder mixture of the precursors (CDP:$CsH_5(PO_4)_2$ = 5:2 molar ratio) was packed into a zirconia rotor for placement into the probe. Variable-temperature ^{1}H and ^{31}P NMR spectra were collected between room temperature and 145 °C. For ^{1}H NMR, a single $\pi/2$-pulse of 5.70 μs was applied with a recycle delay of 500 s. For ^{31}P NMR, a single $\pi/2$-pulse of 2.98 μs was applied with a recycle delay of 1000 s. For measurements taken between 120 and 145 °C, in which the CPP phase was observed, the recycle delay for both ^{1}H and ^{31}P was set to 50 s. In a separate series of measurements, 24-kHz ^{1}H-decoupling was applied during the collection of ^{31}P NMR spectra between room temperature and 120 °C. In the ^{1}H-decoupled ^{31}P NMR measurements, again, a single $\pi/2$-pulse of 2.98 μs was applied but with a 300 s recycle delay. In all measurements, 10 min of temperature equilibration was allowed at each step prior to data acquisition. The ^{31}P NMR shifts were calibrated using 85 wt % H_3PO_4 with a ^{31}P resonance at 0 ppm. The ^{1}H NMR shifts were calibrated using adamantane with a ^{1}H resonance at 1.83 ppm. Temperature control was achieved using a heated dry N_2 gas stream, and temperature values were calibrated using ^{207}Pb NMR of $Pb(NO_3)_2$.

2.2. Results: Structure of $Cs_7(H_4PO_4)(H_2PO_4)_8$. The cubic structure adopted by $Cs_7(H_4PO_4)(H_2PO_4)_8$ (Figure 1a-c, Table 1, and Table S-2) bears significant similarities to that of superprotonic CDP. Like the latter, CPP has a CsCl-like structure with orientationally disordered $H_2PO_4^-$ groups residing on the anion sites. In contrast to CDP, however, one of every eight cation sites of the CsCl substructure is occupied by an orientationally disordered PO_4 group. The regular placement of these groups results in a 4 × 4 × 4 superstructure relative to CDP with a reduced symmetry space group of $Pm\bar{3}n$. Electrostatic considerations argue that these PO_4 groups must be polycations of chemistry $H_4PO_4^+$, a conclusion supported by NMR studies described below. Using these site-charge assumptions, the asymmetric unit contains five Cs cations, two $H_4PO_4^+$ cations (centered around P1 and P2), and two $H_2PO_4^-$ anions (centered around P3 and P4). Because of the high degree of orientational disorder associated with the phosphate groups, it was not possible to resolve the proton positions from the diffraction analysis.

Table 1. Structure of $Cs_7(H_4PO_4)(H_2PO_4)_8$ with Atomic Positions and Site Occupancies[a]

atom	x	y	z	occupancy
Cs1	0.25	0.5	0	1
Cs2	0	0.5	0	1
Cs3	0.25	0.25	0.25	1
Cs4	0	0.23261(6)	0	1
Cs5	0.27088(4)	0.24886(3)	0	1
P1	0	0	0	1
P2	0.5	0.25	0	1
P3	0.13502(8)	0.13502(8)	0.13502(8)	1
P4	0.13421(9)	0.36442(9)	0.11283(9)	1
O1	−0.0517(12)	0.0557(11)	0	1/3
O2	0.086(3)	0.077(2)	0.1237(8)	1/3
O3	0.1974(9)	0.0903(9)	0.1222(18)	1/3
O4	0.1974(7)	0.1299(13)	0.0906(7)	1/3
O5	0.2086(6)	0.1540(14)	0.1397(14)	1/3
O6	0.0902(7)	0.3012(6)	0.1155(13)	1/3
O7	0.1178(11)	0.3028(7)	0.1576(8)	1/3
O8	0.1488(14)	0.2922(6)	0.0952(13)	1/3
O9	0.1979(8)	0.3720(15)	0.1563(8)	1/3
O10	0.1981(8)	0.4078(10)	0.1141(17)	1/3
O11	0.2080(5)	0.3480(10)	0.1004(12)	1/3
O12	0.1242(9)	0.4182(13)	0.1647(13)	1/3
O13	0.0952(14)	0.3781(11)	0.1767(9)	1/3
O14	0.0799(15)	0.4181(15)	0.1234(13)	1/3
O15	0.1214(13)	0.4109(7)	0.0529(7)	1/3
O16	0.0869(7)	0.3724(17)	0.0529(7)	1/3
O17	0.150(2)	0.357(2)	0.0391(8)	1/3
O18	0.4420(8)	0.2005(9)	0	1/3
O19	0.5532(11)	0.3020(11)	0	1/3
O20	0.4463(5)	0.25	−0.0537(5)	1/3

[a]Anisotropic thermal displacements are provided in Table S1. The number in parentheses is the uncertainty in the final digit(s).

The geometric parameters characterizing the PO_4 tetrahedra are summarized in Table S-3. The 1/3 occupancy of oxygen atoms about the P3 and P4 atoms can be readily mapped to three distinct orientations for these anion phosphates (Table S-3). The average P−O bond lengths in these units are 1.552(11) Å (P3) and 1.548(11) Å (P4), in agreement with the values reported for $H_2PO_4^-$ tetrahedra by Ichikawa et al.[26] In the case of the P1 and P2 $H_4PO_4^+$ groups, six orientations are inferred, with each oxygen position being relevant to two unique orientations. The P−O(H) bond lengths of the $H_4PO_4^+$ cations, in which all four P−O bonds are presumed to be protonated, have average values of 1.535(11) Å (P1) and 1.528(15) Å (P2). These bond distances, which are notably shorter than the analogous distances in the polyanion groups,

https://dx.doi.org/10.1021/jacs.0c08870
J. Am. Chem. Soc. 2020, 142, 19992−20001

are consistent with the values of around 1.53 Å reported for $P(OH)_4^+MF_6^-$.[20]

The ^{1}H-decoupled high-temperature ^{31}P NMR spectra, acquired between 110 and 120 °C, Figure 2 and Table S-4,

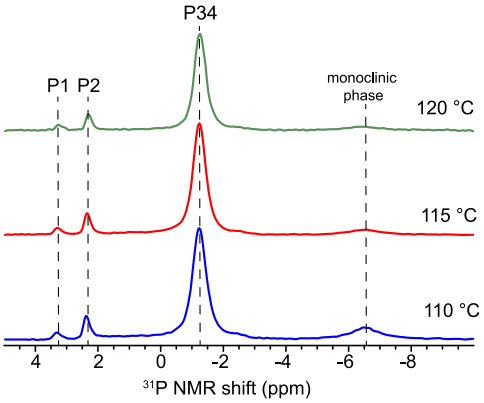

Figure 2. Variable-temperature ^{1}H-decoupled ^{31}P NMR spectra collected between 110 and 120 °C. Peaks p1 and p2 are attributed to the polycations about P1 and P2, respectively, whereas peak p34 is attributed to the polyanions about P3 and P4.

show four distinct phosphorus resonances. The −7 ppm resonance corresponds to the phosphorus signal of monoclinic CDP and diminishes in intensity with increasing temperature as the transformation to CPP reaches completion. The features of the remaining three resonances are largely temperature invariant and are attributed to CPP. The most prominent of these appears at −1.2 ppm and closely matches both the position and the breadth of the phosphorus signal of superprotonic CDP (−1.8 ppm).[27] Thus, we assign this resonance (p34) to the anion-site phosphorus atoms (P3, P4); the chemical environments of these two distinct atoms are apparently too similar to enable their resolution, although there is a hint of a shoulder on the down-shift side of the main peak. The two other phosphorus resonances at 3.3 ppm (p1) and 2.3 ppm (p2) are assigned to the cation-site phosphorus atoms P1 and P2, respectively. The assignment is in agreement with previous ^{31}P NMR studies of $H_4PO_4^+$ cations in concentrated acidic solutions, which reported chemical shifts of approximately 2 ppm relative to phosphoric acid.[22,23,28] A downshift relative to the anion-site phosphorus resonance is also consistent with the expectation that further protonating a phosphate group will draw electron density away from the central P, thereby reducing its electron shielding. The ratio of integrated peak intensities, with p1:p2:p34 = 1:2.91:31.05, closely matches that expected from the structure determination (1:3:32). The sharpness of the p1, p2, and p34 resonances is indicative of the rapid rotation of each phosphate tetrahedra. This motion is further apparent in the XRD refined thermal displacement parameters of the oxygen atoms, which are enlarged in the direction normal to the P−O bonds in comparison to those of the cesium and phosphorus atoms (Figure 1a). The rotation of the $H_4PO_4^+$ polycation creates a relatively isotropic cation, which presumably facilitates its substitutional replacement of Cs^+ in the structure.

The ^{1}H MAS NMR spectra acquired at temperatures at which the CPP phase is stable, between 120 and 145 °C, are shown in Figure 3. The spectra contained only one major resonance centered around 13.4 ppm, which is split into two peaks due to ^{1}H−^{31}P J-coupling of ∼50 Hz. The splitting is

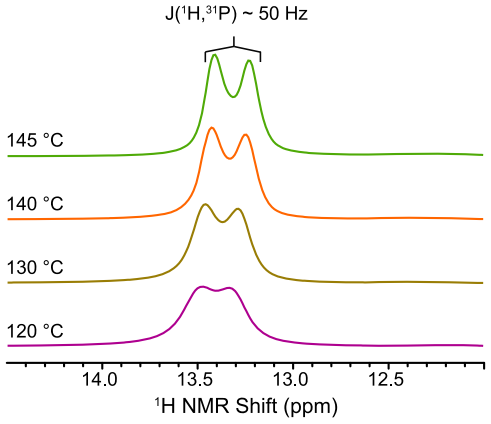

Figure 3. Variable-temperature ^{1}H MAS NMR spectra acquired between 120 and 145 °C. A single split resonance is observed, which is indicative of rapid proton transfer between the polycation and polyanion phosphate groups.

consistent with that of the p1 and p2 resonances in the ^{31}P NMR spectra without ^{1}H-decoupling (Figure S-1). The local chemical environments of the protons on the polycation ($H_4PO_4^+$) and polyanion ($H_2PO_4^-$) groups are undoubtedly distinct, and their differentiation by NMR would be expected. Indeed, the ^{31}P NMR spectra without ^{1}H-decoupling (Figure S-1) show strong ^{1}H−^{31}P coupling only about the p1 and p2 peaks of the polycation phosphorus species. Thus, the single proton resonance indicates rapid proton exchange between all sites, including exchange between polycation and polyanion proton sites. That the individual proton chemical environments cannot be resolved implies that the exchange rate is very fast, estimated to be on the order of 10^8 Hz.

The manner in which the $H_4PO_4^+$ cations are arranged within the CPP structure is of some note, Figure 1d. Within the 4 × 4 × 4 superstructure cell, the polycations reside on the corner and body-centered sites (P1), as well as two sites on each of the unit cell faces (P2). In principle, a simpler arrangement with equivalent stoichiometry can be achieved by placing the $H_4PO_4^+$ cations at the corners of a 2 × 2 × 2 supercell. Adoption of the observed, more complex arrangement may result because it minimizes the extent to which $H_4PO_4^+$ cations interact. In both the hypothetical and the observed arrangements, the shortest distance between $H_4PO_4^+$ cations, which presumably corresponds to the highest energy interaction, is equal to twice the substructure lattice constant ($2a_{sub}$). In the hypothetical 2 × 2 × 2 supercell, each $H_4PO_4^+$ cation is involved in six such interactions. In the observed structure, interactions at this short distance ($2a_{sub}$) are observed only between P2 $H_4PO_4^+$ cations, with each P2 cation neighboring two other P2 species. The second nearest neighbor distances are conversely shorter in CPP (Figure S-2), and an energy minimization argument for the cation arrangement in CPP implies that the interaction energy between $H_4PO_4^+$ cations must drop relatively steeply with distance. It is of some interest to note the Cs2 atom, which lies directly along the short P2−P2 distance, has a displacement ellipsoid that is elongated in the direction of the polycation groups, Figure 1a. We suggest that motion of this Cs atom accommodates the reorientation of the bulky $H_4PO_4^+$ species.

https://dx.doi.org/10.1021/jacs.0c08870
J. Am. Chem. Soc. 2020, 142, 19992−20001

3. PHASE FORMATION AND STABILITY RANGE

3.1. Methods. The high-temperature phase behavior of CPP was investigated using high-temperature X-ray powder diffraction (HTXRD) under both ambient air and active humidification. Samples were prepared by pressing precursor powders of CDP and $CsH_5(PO_4)_2$ (5:2 molar ratio) into thin compacts (~0.1 mm thick, 57 MPA) to enhance interparticle contact and facilitate solid-state reaction. A Rigaku SmartLab Gen 3 9 kW instrument (Cu Kα, 45 kV, 160 mA) equipped with an Anton Paar XRK900 furnace was used for data collection under ambient air. Samples were heated at a ramp rate of 1 °C/min and held at each measurement temperature for 15 min prior to data collection (10° 2θ/min and a 0.1° step size). Patterns were recorded at 10 °C increments between 90 and 140 °C, and again at 5 °C increments in this temperature range on cooling. HTXRD measurements under controlled humidity were performed using an in-house constructed stage,[9] mounted on a Rigaku Ultima diffractometer (Cu Kα, 40 kV, 44 mA). The sample was exposed to a humidified atmosphere (pH_2O = 0.4 atm) at temperatures above 130 °C by introducing 25 sccm of N_2, bubbled through a 80 °C water bath prior to entering the sample chamber. Humidification was introduced only at temperatures above 130 °C to prevent condensation of water vapor in the stage. Data were collected at temperatures between 130 and 165 °C, with a ramp rate of 1 °C/min and a 15 min hold at each temperature prior to data collection (5° 2θ/min and a 0.3° step size).

The thermodynamic properties of CPP were studied by simultaneous thermogravimetric analysis (TGA) and differential scanning calorimetry (DSC) using a Netzsch STA F3 equipped with a water vapor generator. Measurements were performed under nominally dry Ar and under seven different H_2O partial pressures of between 0.05 and 0.6 atm using Ar as a carrier gas (Figure S-1, Figure S-2, and Table S-5). Ground powder samples (50−60 mg) were loaded into a Pt pan and heated at a rate of 1 °C/min. For measurements under humidified atmospheres, the sample was heated to 130 °C and held for 2 h before water vapor was introduced. Again, humidification was applied only at 130 °C and higher so as to avoid water condensation.

3.2. Results: Thermodynamics of CPP Formation. The HTXRD data (Figure 4) and thermal analysis results (Figure 5) reveal that CDP and $CsH_5(PO_4)_2$ react at elevated temperatures to form CPP. Specifically, the diffraction data show retention of the two reactant phases at 90 °C, whereas at 110 °C only CPP is observed. The DSC profile reveals that this structural change is accompanied by a distinct thermal event that initiates at 90 °C (and completes by ~110 °C). Notably, no weight loss is observed during the DSC transition, consistent with a solid-state transformation. The temperature (T_{rxn}), enthalpy ($\Delta_{rxn}H$), and entropy ($\Delta_{rxn}S = \Delta_{rxn}H/T_{rxn}$) of the reaction were found to be 89.5 ± 1.2 °C, 47 ± 5 kJ/mol, and 130 ± 14 J/mol·K, Table 2, respectively, as averaged over eight measurements, Figure S-4.

Further heating beyond the reaction temperature resulted in conventional thermal expansion behavior (thermal expansion coefficient $\alpha = 3.8(9) \times 10^{-5}$ K^{-1}, a = 20.2032(2) Å at 130 °C, Figure S-3). Retention of CPP was observed in the diffraction data collected in the absence of active humidification up to 140 °C, Figure 4, and the onset of CPP decomposition at 151 °C was evident in coincident mass loss and endothermic events (Figure 5). Thus, CPP is stable over a large temperature window (90−151 °C) in nominally dry conditions. This stands in marked contrast to CDP, the only other compound with a superprotonic phase composed of oxyanions that are solely

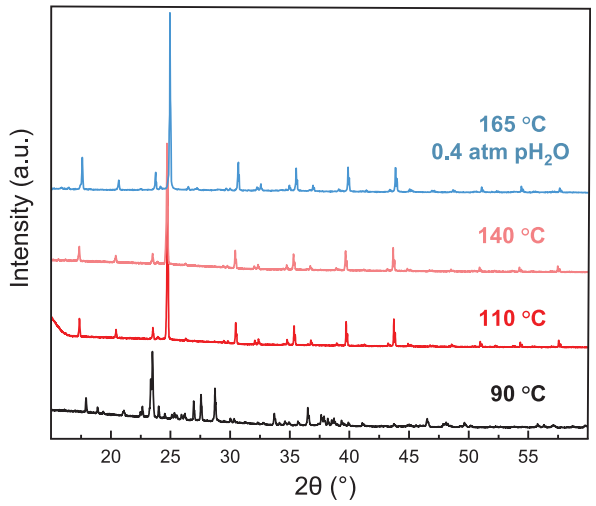

Figure 4. Powder X-ray diffraction patterns collected at 90, 110, and 140 °C under ambient atmosphere, and at 165 °C under 0.4 atm pH_2O. The pattern collected at 90 °C is a superposition of the patterns of the monoclinic phases of CsH_2PO_4 and $CsH_5(PO_4)_2$. Patterns at 110, 140, and 165 °C are fully indexed to cubic $Cs_7(H_4PO_4)(H_2PO_4)_8$.

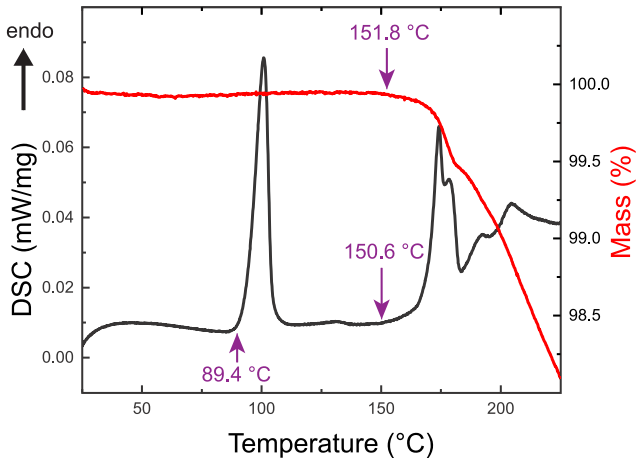

Figure 5. Differential scanning calorimetry and thermogravimetric profiles collected from a 5:2 CDP:$CsH_5(PO_4)_2$ sample heated at 1 °C/min under flowing dry Ar. Here, the DSC peaks for the superprotonic reaction (89 °C) and decomposition (151 °C) frame the stability window of $Cs_7(H_4PO_4)(H_2PO_4)_8$ under nominally dry conditions.

Table 2. Thermodynamic Quantities for the Reaction to Form CPP from the Precursors CDP and $CsH_5(PO_4)_2$[a]

	$Cs_7(H_4PO_4)(H_2PO_4)_8$	normalized per cube	CsH_2PO_4
reaction/transition T (°C)	90.0(1.2)		228
enthalpy (kJ/mol)	48(4)	6.0(5)	11.5
entropy (J/mol·K)	132(11)	16.5(1.4)	22.9

[a]The number in parentheses is the standard deviation in the final digit(s). Values for the superprotonic transition of CDP are provided for comparison.[9]

https://dx.doi.org/10.1021/jacs.0c08870
J. Am. Chem. Soc. 2020, 142, 19992−20001

PO_4 groups, which has a superprotonic phase with a negligible window of stability under dry conditions.

Active humidification resulted in suppression of the mass loss reaction, as evidenced in the differential mass loss curves of Figure 6. Such behavior implies the decomposition occurs by dehydration, typical of this general class of materials. Diffraction data collected at 165 °C under 0.4 atm pH_2O, Figure 4, confirmed retention of the cubic CPP phase to this higher temperature. Close examination of the DSC curves of Figure 6 reveals that those collected with $pH_2O \leq 0.5$ atm are characterized by two overlapping thermal anomalies in the vicinity of the onset of mass loss. The first produces a sharp DSC peak at an onset temperature of 180 °C that is relatively insensitive to humidification and that can be seen to occur without mass loss in the data collected at pH_2O = 0.6 atm. Accordingly, this signal is tentatively assigned to a solid-state phase transition. The second is a broad peak that coincides with the broad peak in the dTG curves. Both of these broad peaks shift to higher temperatures and diminish in intensity with increasing pH_2O. At pH_2O = 0.5 atm, the broad DSC peak is barely visible, whereas at pH_2O = 0.05 it is the dominant thermal event and even initiates at a temperature lower than the apparent solid-state transition. On the basis of these results, a proposed phase stability diagram for $Cs_7(H_4PO_4)(H_2PO_4)_8$ is presented in Figure 7. Here the dehydration temperature is defined using the onset of the dTG mass loss signal, and the solid-state phase transition temperature is defined from the onset of the sharp DSC signal. Decomposition leading to a liquid dehydrate is proposed on the basis of the nature of the product obtained from the thermal analysis experiments, which had the appearance of a vitrified droplet.

4. CONDUCTIVITY

4.1. Methods. Conductivity measurements were made by ac impedance spectroscopy using an Agilent 4284A LCR analyzer. Data were collected using a 20 mV amplitude (under zero bias) over a 10^5−20 Hz frequency range. A dense compact, 1 mm in thickness, was prepared by pressing mixed powders of CDP and $CsH_5(PO_4)_2$ (5:2 molar ratio) in a 15 mm die to achieve 93% theoretical density. Electrodes were applied by sputtering 100 nm of Ag on each side. Data were collected under flowing N_2 (40 sccm) over the temperature range 60−170 °C. At temperatures of 140 °C and higher, the supply gas was humidified by bubbling through a water bath at 80 °C to achieve pH_2O = 0.4 atm. The sample was heated at a rate of 2 °C/min in 5−10 °C increments and was held at each temperature for 30 min prior to measurement.

Impedance spectra were analyzed using the commercial software package Zview. As is typical of solid acid proton conductors,[1] at low temperatures, the spectra displayed a semicircular arc in the Nyquist representation and could be simulated using a single RQ parallel circuit, where R is a resistor (equal to the bulk electrolyte resistance) and Q is a constant phase element ($Z_Q = Q_0^{-1}(i\omega)^{-n}$, where Q_0 is a constant, i is $\sqrt{-1}$, ω is frequency, and n is a constant between 0 and 1).[29] Despite the composite nature of the material, the impedance arc was rather ideal, consistently displaying an n value of ∼0.9. At high temperatures, the characteristic frequency for proton transport exceeded the frequency range of the impedance analyzer, again a typical feature of solid acid superprotonic materials, and a linear response reflecting the electrode was obtained in the Nyquist plot (Figure S-5). These

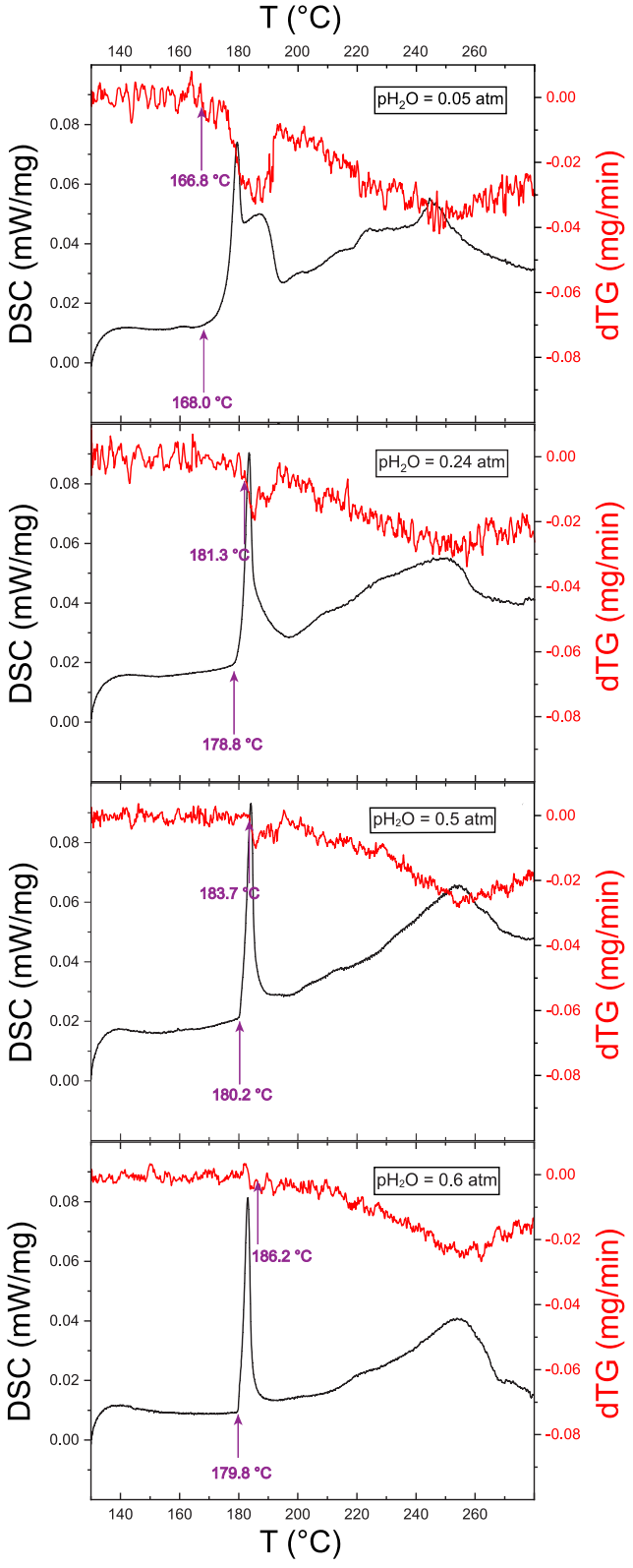

Figure 6. Differential scanning calorimetry and differential thermogravimetric profiles collected from $Cs_7(H_4PO_4)(H_2PO_4)_8$ (formed in situ by reaction between stoichiometric quantities of CDP and $CsH_5(PO_4)_2$) at a heating rate of 1 °C/min under flowing humidified Ar with water vapor partial pressure of (a) 0.05 atm; (b) 0.24 atm; (c) 0.5 atm; and (d) 0.6 atm, revealing the decomposition characteristics of $Cs_7(H_4PO_4)(H_2PO_4)_8$ as well as an unidentified solid-state phase transformation at an onset temperature of 180 °C.

https://dx.doi.org/10.1021/jacs.0c08870
J. Am. Chem. Soc. 2020, 142, 19992−20001

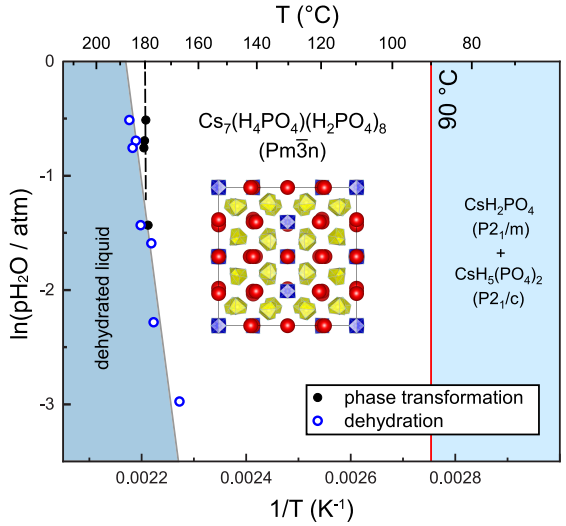

Figure 7. Phase diagram for $Cs_7(H_4PO_4)(H_2PO_4)_8$. Dehydration temperatures are identified according to the onset of mass loss detected in the dTG profile. Phase transformation temperatures are identified according to the onset of the sharp DSC signal, limited to measurements with $pH_2O \geq 0.24$ atm.

spectra were described using a Warburg diffusion element in series with a resistor, where the latter was taken as the bulk electrolyte resistance. Conductivity values were calculated using the fitted resistances and the sample dimensions, which were unchanged after measurement.

4.2. Results. The conductivity values as measured in two successive heating cycles are plotted in Arrhenius form in Figure 8. In the first heating cycle, a dramatic increase in conductivity between 90 and 110 °C due to the formation of CPP is evident, with the conductivity rising in this narrow temperature regime by about 3 orders of magnitude. Following the formation of the CPP phase, the conductivity is linear in the Arrhenius representation, with an activation energy for charge transport of 0.652(4) eV (62.9(4) kJ/mol). In both the subsequent cooling (not shown) and the second heating stages, the data followed the first cycle linear trend for temperatures ranging between 90 and 170 °C. No drop in conductivity corresponding to a reverse transition was observed on cooling. Introduction of humidification during the second heating cycle had no impact of the magnitude of the conductivity, but acted to prevent dehydration and enabled measurement to ~170 °C.

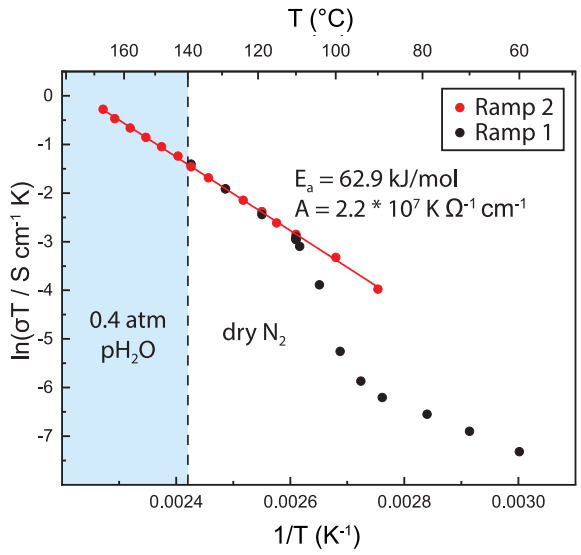

Figure 8. Conductivity of $Cs_7(H_4PO_4)(H_2PO_4)_8$ as measured over two successive heating cycles and plotted in Arrhenius form. The solid line is a fit to the measured data, from which the activation energy and pre-exponential factor for proton transport in $Cs_7(H_4PO_4)(H_2PO_4)_8$ were determined.

Significantly, despite the many similarities between CPP and superprotonic CDP, the activation energy for proton transport of the new material is substantially larger than that of CDP (0.652 vs 0.398 eV).[9] Concomitantly, the conductivity of CPP is lower, although some of the difference is attributable to the lower temperatures at which CPP is stable in comparison to superprotonic CDP. Nevertheless, at 170 °C, close to the high-temperature limit at which CPP is stable under moderate humidification (T = 180 °C, pH_2O = 0.4 atm), the conductivity is ~2 × 10^{-3} S cm^{-1}, an order of magnitude lower than that of CDP at 250 °C.[9] The key structural feature shared between CPP and CDP is the presence of orientationally disordered $H_2PO_4^-$ anion groups, which participate, presumably in both compounds, in the Grotthuss mechanism of proton transport. The key distinction is the presence of $H_4PO_4^+$ cations in CPP, implying that this species must be responsible, either directly or indirectly, for the lower proton conductivity in this material. The ^1H NMR spectra, as discussed above (Figure 3), reveal that fast exchange between polyanion and polycation protons occurs, indicating that long-range proton motion involves the unusual polycation species. Furthermore, as was also noted above, strong $^1H-^{31}P$ coupling is observed about the phosphorus atoms in the polycation groups (Figure S-1), but not those in the polyanion groups. This distinction indicates stronger H−P chemical interactions for the polycation groups than for the polyanion groups, which may in turn reflect a longer mean residence time for protons at the polycation sites (than at the polyanion sites). The participation of the polycations may thus directly impact long-range proton transport by effectively creating proton trapping sites.

Several indirect impacts of the polycation species may also contribute or even be the primary cause of the diminished conductivity and high activation energy in CPP. In CDP, molecular dynamics simulations have pointed to PO_4 reorientation as the rate-limiting step for proton transport.[30] In CPP, the presence of somewhat anisotropic $H_4PO_4^+$ cations with probable hydrogen bonds to the polyanions, and/or the apparently fewer number of accessible polyanion orientations (3 vs 6), may plausibly suppress the reorientation rate. On the other hand (or perhaps in conjunction), a minimum in the potential well for polyanion rotation that is broader than in CDP could result in a decrease in the zero point energy of this unit and thereby an increase in activation energy. Alternatively, the larger distance between polyanion groups ($a_{CPP} > 4\ a_{CDP}$) may render the proton transfer between these units unfavorable such that this step becomes rate-limiting. The structural and macroscopic transport measurements reported here set the stage for a future focused mechanistic study.

5. DISCUSSION OF CPP PHASE FORMATION

The formation of a stable compound that bears the $H_4PO_4^+$ cation is surprising. The rarity of previous observations of this cation suggests that this species is energetically unfavorable. At

https://dx.doi.org/10.1021/jacs.0c08870
J. Am. Chem. Soc. 2020, 142, 19992−20001

first glance, one might assume CPP to be stabilized by the high degree of rotational disorder on both anion and cation sites, particularly because the compound forms at temperatures below which the analogous cubic phase of CDP exists. However, the entropy of the reaction to form CPP is moderate in comparison, for example, to the entropy of the superprotonic transition of CDP, Table 2. In both cases, phase formation and superprotonic transition, the reactants display near-zero orientational disorder in their respective poly-ion groups, and thus the transition/reaction entropy can be largely attributed to the rotational disorder in the high-temperature state.[31] The moderate entropy of CPP appears to result from the limited number of orientations of the $H_2PO_4^-$ anion groups in this compound, only three, as opposed to the six orientations that occur in CDP. Ruling out entropy as the driving factor, the ready formation of CPP must be a consequence of enthalpic considerations. As shown in Table 2, the enthalpy of the reaction is small, approximately one-half that of the enthalpy of the superprotonic transition of CDP, implying that the enthalpy penalty to form CPP is low. The presence of the energetically unfavorable $H_4PO_4^+$ cation in CPP suggests that the enthalpy of formation of CPP (from the elements) must be at least as high, if not higher, than that of superprotonic CDP. Thus, we propose that the low reaction enthalpy is a consequence of a high enthalpy of formation of the reactant, $CsH_5(PO_4)_2$. This interpretation is supported by the observation that $CsH_5(PO_4)_2$ decomposes/melts at a relatively low temperature of ~130 °C under inert atmosphere (Figure S-7). In contrast, CDP under similar conditions is stable to ~224 °C.[32] Schematic diagrams of the thermodynamic relations underlying the arguments presented here are given in Figure S-8 (derivatives of Hess law diagrams) along with further discussion. Finally, we note that, although the reverse transformation was not extensively studied, in no case was a low symmetry form of CPP encountered. Instead, a gradual return to the precursor compounds occurred.

6. CONCLUSION AND SUMMARY

The structure, thermodynamic, and proton transport properties of superprotonic $Cs_7(H_4PO_4)(H_2PO_4)_8$ (CPP), a new compound, are presented in this work. The compound forms at 90 °C from the reaction of CDP and $CsH_5(PO_4)_2$. Single-crystal diffraction studies in concert with NMR spectroscopy revealed rotationally disordered $H_4PO_4^+$ polycations as periodic features on the cation lattice, replacing Cs on one of every eight cation sites. The regular, periodic placement of the $H_4PO_4^+$ cations reduces the symmetry of the cubic structure to $Pm\bar{3}n$ from the ideal $Pm\bar{3}m$ space group of the CsCl structure type and creates a 4 × 4 × 4 supercell of cubic CDP-like unit cells. The occurrence of CPP, with the enthalpically unfavorable $H_4PO_4^+$ unit, is proposed to be the consequence of a high enthalpy of formation of $CsH_5(PO_4)_2$, as opposed to a high entropy of formation of CPP. The low formation temperature contributes to the wide window of thermal stability of CPP, which extends under nominally dry conditions up to ~151 °C. This phase behavior stands in contrast to that of CDP, the only other superprotonic solid acid formed of entirely phosphate polyanion groups, which has a negligible window of stability in the superprotonic phase under nominally dry conditions. Despite the high degree of polyanion disorder in CPP and its overall structural similarity to CDP, the activation energy for proton transport is high and the conductivity is moderate. This is an apparent consequence of the participation of the polycation groups in the long-range proton transport. Thus, in terms of the application of CPP as an electrolyte, it remains to be seen whether the advantages offered, operation at reduced temperatures without the requirement of active humidification, can outweigh the advantages of high conductivity and higher operating temperatures offered by CDP and other inorganic proton conductors such as SnP_2O_7 and analogues.[33]

■ ASSOCIATED CONTENT

Supporting Information

The Supporting Information is available free of charge at https://pubs.acs.org/doi/10.1021/jacs.0c08870.

Table S-1, Single-crystal diffraction, structure solution, and refinement details; Table S-2, Structure of $Cs_7(H_4PO_4)(H_2PO_4)_8$ with atomic positions, site occupancy, and anisotropic thermal displacement parameters; Table S-3, P−O bond length and O−P−O bond angles for (a) P1, (b) P2, (c) P3, and (d) P4; Table S-4, ^{31}P NMR details for the resonances in each scan temperature; Figure S-1, Comparison of ^{31}P MAS NMR spectra of $Cs_7(H_4PO_4)(H_2PO_4)_8$ collected at 120 °C with and without ^1H-decoupling; Figure S-2, Analysis of the $H_4PO_4^+$−$H_4PO_4^+$ interactions in (a) the CPP structure versus (b) the hypothetical 2 × 2 × 2 supercell structure; Table S-5, Ar and water vapor flow rates for various humidified atmospheres in TGA/DSC measurements; Figure S-3, Lattice parameter of $Cs_7(H_4PO_4)(H_2PO_4)_8$ as a function of temperature; Figure S-4, Superprotonic reaction DSC peaks, which were averaged to obtain thermodynamic values for the reaction; all samples were heated at 1 °C/min under dry Ar atmosphere; Figure S-5, DSC signal from a measurement in which the (CDP + $CsH_5(PO_4)_2$) sample was heated to 130 °C, cooled to 25 °C, held for 3 h, and then heated to 130 °C again; Figure S-6, Representative impedance spectra for the (a) low-temperature and (b) high-temperature responses of $Cs_7(H_4PO_4)(H_2PO_4)_8$; impedance values have been normalized to the thickness and area of the pellet; note the 3 order-of-magnitude difference in the scale between the low- and high-temperature responses; low-temperature spectra with semicircular arcs were fit using RQ circuits; high-temperature spectra were fit using a Warburg diffusion element; Figure S-7, TGA/DSC measurement of $CsH_5(PO_4)_2$ with a ramp rate of 1 °C/min under a flow of 20 sscm Ar; and Figure S-8, Schematic of proposed formation Gibbs free energies, enthalpies, and entropies for the CsH_2PO_4−$CsH_5(PO_4)_2$ phase space (PDF)

X-ray crystallographic data for $Cs_7(H_4PO_4)(H_2PO_4)_8$ (CIF)

■ AUTHOR INFORMATION

Corresponding Author

Sossina M. Haile − *Materials Science & Engineering, Northwestern University, Evanston, Illinois 60208, United States;* orcid.org/0000-0002-5293-6252; Email: sossina.haile@northwestern.edu

https://dx.doi.org/10.1021/jacs.0c08870
J. Am. Chem. Soc. 2020, 142, 19992−20001

Authors

Louis S. Wang − *Materials Science & Engineering, Northwestern University, Evanston, Illinois 60208, United States;* orcid.org/0000-0003-4046-2341

Sawankumar V. Patel − *Department of Chemistry & Biochemistry, Florida State University, Tallahassee, Florida 32306-4390, United States;* orcid.org/0000-0002-5293-9330

Sheel S. Sanghvi − *Materials Science & Engineering, Northwestern University, Evanston, Illinois 60208, United States*

Yan-Yan Hu − *Department of Chemistry & Biochemistry, Florida State University, Tallahassee, Florida 32306-4390, United States;* orcid.org/0000-0003-0677-5897

Complete contact information is available at: https://pubs.acs.org/10.1021/jacs.0c08870

Notes

The authors declare no competing financial interest.

■ ACKNOWLEDGMENTS

Financial support has been provided by the National Science Foundation (DMR 1807234 and DGE-1842165). Single-crystal XRD experiments made use of the Integrated Molecular Structure Education and Research Center (IMSERC) at Northwestern University, which is supported by the Soft and Hybrid Nanotechnology Experimental (SHyNE) Resource (NSF ECCS-1542205, the State of Illinois, and International Institute for Nanotechnology (IIN)). We thank Charlotte Stern and Christos Malliakas for single-crystal data collection and discussion on structure refinement. This work made use of the J. B. Cohen X-ray Diffraction facility at NU, supported by the NSF MRSEC program (NSF DMR-1720139), and we thank Jerry Carsello for his years assisting our experiments as facility manager.

■ REFERENCES

(1) Haile, S. M.; Chisholm, C. R. I.; Sasaki, K.; Boysen, D. A.; Uda, T. Solid Acid Proton Conductors: From Laboratory Curiosities to Fuel Cell Electrolytes. *Faraday Discuss.* **2007**, *134*, 17−39.

(2) Uda, T.; Haile, S. M. Thin-Membrane Solid-Acid Fuel Cell. *Electrochem. Solid-State Lett.* **2005**, *8* (5), 245−246.

(3) Chisholm, C. R. I.; Boysen, D. A.; Papandrew, A. B.; Zecevic, S.; Cha, S.; Sasaki, K. A.; Varga, A.; Giapis, K. P.; Haile, S. M. From Laboratory Breakthrough to Technological Realization: The Development Path for Solid Acid Fuel Cells. *Electrochem. Soc. Interface* **2009**, *18*, 53−59.

(4) Lim, D. K.; Liu, J.; Pandey, S. A.; Paik, H.; Chisholm, C. R. I.; Hupp, J. T.; Haile, S. M. Atomic Layer Deposition of Pt@CsH2PO4 for the Cathodes of Solid Acid Fuel Cells. *Electrochim. Acta* **2018**, *288*, 12−19.

(5) Papandrew, A. B.; Chisholm, C. R. I.; Elgammal, R. A.; Özer, M. M.; Zecevic, S. K. Advanced Electrodes for Solid Acid Fuel Cells by Platinum Deposition on CsH2PO4. *Chem. Mater.* **2011**, *23* (7), 1659−1667.

(6) Uda, T.; Boysen, D. A.; Chisholm, C. R. I.; Haile, S. M. Alcohol Fuel Cells at Optimal Temperatures. *Electrochem. Solid-State Lett.* **2006**, *9* (6), A261.

(7) Boysen, D. A.; Uda, T.; Chisholm, C. R. I.; Haile, S. M. High-Performance Solid Acid Fuel Cells Through Humidity Stabilization. *Science (Washington, DC, U. S.)* **2004**, *303* (5654), 68−70.

(8) Ikeda, A.; Haile, S. M. The Thermodynamics and Kinetics of the Dehydration of CsH2PO4 Studied in the Presence of SiO2. *Solid State Ionics* **2012**, *213*, 63−71.

(9) Ikeda, A.; Kitchaev, D. A.; Haile, S. M. Phase Behavior and Superprotonic Conductivity in the Cs 1-XRbxH2PO4 and Cs 1-XKxH2PO4 Systems. *J. Mater. Chem. A* **2014**, *2* (1), 204−214.

(10) Baranov, A. I.; Dolbinina, V. V.; Lanceros-Mendez, S.; Schmidt, V. H. Phase Diagram and Dielectric Properties of Mixed Cs1-X(NH 4)XH2PO4 Crystals. *Ferroelectrics* **2002**, *272* (November 2014), 225−230.

(11) Ponomareva, V. G.; Bagryantseva, I. N.; Shutova, E. S. Effect of Cation Substitution in Cs1−2xBaxH2PO4 on Structural Properties and Proton Conductivity. *Phys. Solid State* **2017**, *59* (7), 1387−1394.

(12) Ponomareva, V. G.; Bagryantseva, I. N. The Influence of Cs2HPO4·H2O Impurity on the Proton Conductivity and Thermal Properties of CsH2PO4. *Solid State Ionics* **2019**, *329* (December 2018), 90−94.

(13) Ponomareva, V. G.; Bagryantseva, I. N. Proton Conductivity, Structural and Thermal Properties of (1−x) CsH 2 PO 4 − xBa(H 2 PO 4) 2. *Phys. Solid State* **2017**, *59* (9), 1829−1835.

(14) Mohammad, N.; Mohamad, A. B.; Kadhum, A. A. H.; Loh, K. S. Effect of Silica on the Thermal Behaviour and Ionic Conductivity of Mixed Salt Solid Acid Composites. *J. Alloys Compd.* **2017**, *690*, 896−902.

(15) Yoshimi, S.; Matsui, T.; Kikuchi, R.; Eguchi, K. Temperature and Humidity Dependence of the Electrode Polarization in Intermediate-Temperature Fuel Cells Employing CsH2PO4/SiP2O7-Based Composite Electrolytes. *J. Power Sources* **2008**, *179* (2), 497−503.

(16) Oh, S. Y.; Kawamura, G.; Muto, H.; Matsuda, A. Mechanochemical Synthesis of Proton Conductive Composites Derived from Cesium Dihydrogen Phosphate and Guanine. *Solid State Ionics* **2012**, *225*, 223−227.

(17) Ponomareva, V. G.; Lavrova, G. V. Effect of the Excess Protons on the Electrotansport, Structural and Thermodynamic Properties of CsH2PO4. *Solid State Ionics* **2017**, *304*, 90−95.

(18) Arlman, E. J. The Basic Properties of Orthophosphoric Acid. *Recl. des Trav. Chim. des Pays-Bas* **1937**, *56* (10), 919−922.

(19) Mathew, M.; Wong-Ng, W. Crystal Structure of a New Monoclinic Form of Potassium Dihydrogen Phosphate Containing Orthophosphacidium Ion, (H4PO4)+1. *J. Solid State Chem.* **1995**, *114*, 219−223.

(20) Minkwitz, R.; Schneider, S. Synthesis and Characterization of the Tetra- Hydroxyphosphonium Hexafluorometalates. *Angew. Chem., Int. Ed.* **1999**, *218* (1), 210−212.

(21) Gillespie, R. J.; Robinson, E. A. The Sulfuric Acid Solvent System. *Adv. Inorg. Chem. Radiochem.* **1959**, *1* (C), 385−423.

(22) Addison, C. C.; Bailey, J. W.; Bruce, S. H.; Dove, M. F. A.; Hibbert, R. C.; Logan, N. Chemistry in Fuming Nitric Acids—I. NMR Spectroscopic Study of PF5, HPO2F2 and P4O10 in the Solvent System 44 Wt.% N2O4 in 100% HNO3. *Polyhedron* **1983**, *2* (7), 651−656.

(23) Hibbert, R. C.; Logan, N. Multinuclear Nuclear Magnetic Resonance Study of the Interaction of Some Phosphorus(V) Compounds with Inorganic Acids. The Protonating Abilities of HNO3, MeSO3H, and HPO2F2 towards the Phosphoryl Group. *J. Chem. Soc., Dalton Trans.* **1985**, 865−866.

(24) Sanghvi, S. S. *Superprotonic Solid Acids: Structure and Discovery*; Northwestern University, 2019.

(25) Sheldrick, G. M. A Short History of SHELX. *Acta Crystallogr., Sect. A: Found. Crystallogr.* **2008**, *64* (1), 112−122.

(26) Ichikawa, M. Dependence of the Distortion of the Tetrahedra in Acid Phosphate Groups HnPO4 (N= 1−3) on Hydrogen-Bond Length. *Acta Crystallogr., Sect. B: Struct. Sci.* **1987**, *43* (No. 43), 23−28.

(27) Kim, G.; Blanc, F.; Hu, Y. Y.; Grey, C. P. Understanding the Conduction Mechanism of the Protonic Conductor CsH 2PO4 by Solid-State NMR Spectroscopy. *J. Phys. Chem. C* **2013**, *117* (13), 6504−6515.

(28) Dillon, K. B.; Waddington, T. C. Behavior of Some Inorganic Phosphates in Strongly Acidic Solvents Studied by Phosphorus-31

Nuclear Magnetic Resonance Spectroscopy. *J. Chem. Soc. A* **1970**, No. No. 0, 1146−1150.
(29) Boukamp, B. A. Electrochemical Impedance Spectroscopy in Solid State Ionics: Recent Advances. *Solid State Ionics* **2004**, *169*, 65−73.
(30) Lee, H. S.; Tuckerman, M. E. The Structure and Proton Transport Mechanisms in the Superprotonic Phase of CSH2PO4: An Ab Initio Molecular Dynamics Study. *J. Phys. Chem. C* **2008**, *112* (26), 9917−9930.
(31) Chisholm, C. R. I.; Haile, S. M. Entropy Evaluation of the Superprotonic Phase of CsHSO4: Pauling's Ice Rules Adjusted for Systems Containing Disordered Hydrogen-Bonded Tetrahedra. *Chem. Mater.* **2007**, *19* (2), 270−279.
(32) Boysen, D. A.; Haile, S. M.; Liu, H.; Secco, R. A. High-Temperature Behavior of CsH2PO4 under Both Ambient and High Pressure Conditions. *Chem. Mater.* **2003**, *15* (3), 727−736.
(33) Sato, Y.; Shen, Y.; Nishida, M.; Kanematsu, W.; Hibino, T. Proton Conduction in Non-Doped and Acceptor-Doped Metal Pyrophosphate (MP 2O 7) Composite Ceramics at Intermediate Temperatures. *J. Mater. Chem.* **2012**, *22* (9), 3973−3981.

https://dx.doi.org/10.1021/jacs.0c08870
J. Am. Chem. Soc. 2020, 142, 19992−20001